Melting curves of metals with excited electrons in the quasiharmonic approximation

D. V. Minakov
Joint Institute for High Temperatures, Izhorskaya 13 Bldg 2, Moscow 125412, Russia
and Moscow Institute of Physics and Technology, 9 Institutskiy per., Dolgoprudny, Moscow Region, 141700, Russia

P. R. Levashov
Joint Institute for High Temperatures, Izhorskaya 13 Bldg 2, Moscow 125412, Russia
and Tomsk State University, 36 Lenin Prospekt, Tomsk 634050, Russia

(Received 3 September 2015; revised manuscript received 28 October 2015; published 7 December 2015)

We present melting curves of aluminum, copper, and nickel calculated on the basis of a quasiharmonic approximation. The dependence of a phonon density of states on electron temperature is taken into account for both thermodynamic properties and a mean square displacement of atoms. Linear expansion coefficients are strongly dependent on an approximation of the exchange-correlation functional; the generalized gradient approximation gives better results at normal conditions. Using the Lindemann criterion we obtain good agreement with experimental pressure dependences of the melting temperature for Al and Cu. In the case of Ni we consider a spin polarization effect to reproduce a recent first-principle simulation and shock-wave data. However, our melting curve is located significantly higher than static experimental points. We also consider a thermal excitation of electrons in a crystal and investigate the dependence of the melting temperature on the electronic one at normal and elevated densities. Hardening of the crystal structure for all the metals is obtained in our simulation; this effect might be confirmed experimentally owing to a relatively long lifetime of the two-temperature state.

DOI: 10.1103/PhysRevB.92.224102 PACS number(s): 64.70.D−, 63.20.−e, 79.20.Ds, 71.15.Mb

I. INTRODUCTION

Prediction of melting curves of metals is a complicated theoretical problem with a long history. To describe the phenomenon of melting, two approaches are usually used [1]. In the two-phase method Gibbs potentials of liquid and solid phases are compared with each other. The equality of the potentials at the same pressure and temperature gives the conditions of melting. Theoretically it is a complicated task as accurate equations of state (EOS) of every phase should be known. On the other hand, a direct molecular simulation of melting is possible: The liquid and solid phases coexist in the same computational cell ensuring the validity of the melting conditions [2]. Unfortunately in a classical molecular dynamics (MD) simulation the result is determined by an interparticle potential which is unknown under high pressures and temperatures. On the other hand, the quantum molecular dynamics (QMD) can deal with only about 1000 particles so in this case it is quite difficult to obtain equilibrium; moreover, such computations are very time consuming.

The second approach, the one-phase method, considers the conditions under which a crystal becomes unstable [3] and thus melts. A number of approximate melting criteria can be applied in this case. The Lindemann criterion [4] was introduced more than 100 years ago and is widely used up to now. The modern formulation of this criterion was given by Gilvarry on the basis of the Debye model [5]. The generalized version of the Lindemann criterion [6] is able to confirm the well-known empirical Simon rule [7] and the Kraut-Kennedy melting law [8]. It was also shown [9] that the Lindemann criterion is exact for a purely repulsive potential of the form $\phi(\mathbf{r}) \sim \mathbf{r}^{-n}$. This result is a rigorous consequence of the scaling properties of potentials which are homogeneous in the coordinates of all atoms [3,9,10]. The validity of the Lindemann criterion was investigated by many authors. It is known that the Lindemann parameter is almost constant for metals with the same crystal structure (for example, 0.1–0.13 for fcc metals) [11]. This is the consequence of the fact that the interaction in the elemental metals may be reasonably represented by the potential of the form $\phi(r) = \varepsilon\phi(r/\sigma)$ with a common shape function ϕ but different ε and σ parameters. For minerals, however, the interaction is more complex so a simple homogeneous two-parameter potential is invalid; in this case the Lindemann criterion may fail [12].

Experiments on the femtosecond laser irradiation of metals raised a question about the properties of a crystal with the heated electron subsystem. Different temperatures of the electrons and the lattice may significantly influence thermodynamic [13–15] and transport [16–20] properties of metals. For example, there is indirect experimental evidence of the gold crystal hardening under the femtosecond laser heating [21]. On the other hand, excitation of electrons in the crystal of tungsten up to temperatures between 1.7 and 4.3 eV causes the instability of the bcc structure and may result in the so-called nonthermal transition to the fcc or hcp phase [22]. To investigate these effects a quasiharmonic approximation (QA) is usually applied. This method studies small oscillations of atoms in a crystal about their equilibrium positions. The QA allows one to calculate phonon dispersion curves, a phonon density of states (PhDOS) and thermodynamic properties [23–25]. Using the PhDOS it is possible to compute a mean square displacement of the atoms [26]. Then the Lindemann criterion enables one to compute the melting curve as it was previously demonstrated for sodium [27]. The other advantage of the QA is the ability to investigate a system with different temperatures of the electrons and the lattice due to the adiabatic (Born-Oppenheimer) approximation. It was predicted earlier [28] that for an abstract bcc metal the melting temperature would slightly rise with the electronic one. Later it was shown using *ab initio* methods that for

gold [13] this effect is quite significant. In this work we apply the QA to obtain the melting curves of aluminum, copper and nickel at different compressions and electronic temperatures. We take into account the thermal expansion of the crystal as well as the dependence of the PhDOS on the electronic temperature. However, we neglect the anharmonic effects. The obtained results on the melting curves of Al and Cu demonstrate excellent agreement with experiment. Also, the account of a spin polarization for Ni shifts the melting curve significantly to lower temperatures. We demonstrate the nonmonotonic dependences of the melting temperature vs the electronic one for all the metals.

The paper is organized as follows. In Sec. II we describe our computational method and discuss its specific parameters. Section III contains linear expansion coefficients, melting curves, and melting temperatures at heated electrons for Al, Cu, and Ni. The discussion is presented in Sec. IV. Our conclusion is formulated in the last section.

II. METHODS AND PARAMETERS OF CALCULATIONS

We used the plane-wave pseudopotential VASP code [29–32] to calculate the electronic structure of a crystal in the framework of the density functional theory (DFT) and the PHONOPY code [33] to obtain the phonon properties. For a chosen supercell the VASP code determines the Hessian matrix using the density functional perturbation theory (DFPT) [34], and then the PHONOPY code calculates the phonon frequencies from the force constants obtained by VASP.

In DFT calculations we used the generalized gradient approximation (GGA) with the Perdew-Burke-Ernzerhof (PBE) [35,36] corrections for the exchange-correlation functional. We also employed the projector-augmented wave (PAW) [37] pseudopotentials in which the expansion of the self-energy in terms of the single particle Green's function and the screened Coulomb interaction is truncated after the first term (the so-called GW approximation) [38]. The following numbers of valence electrons were taken into account: 3 for Al, 11 for Cu and 10 for Ni. Other electrons were included into an invariable core. The Fermi smearing for occupancies was applied in all computations. A spin polarization was considered for Ni in order to correctly describe thermodynamic properties of this metal.

All calculations were performed for an fcc supercell containing 32 atoms. We used a $8 \times 8 \times 8$ k-point mesh with the Monkhorst-Pack [39] generation scheme for the electronic structure and a $61 \times 61 \times 61$ q-point mesh for the phonon properties. A cutoff energy for the plane-wave basis was equal to 700 eV for all the metals.

In the framework of the QA the Helmholtz free energy F of a crystal can be decomposed into the sum of three independent parts:

$$F(V,T_i,T_e) = E_0(V) + F_e(V,T_e) + F_{ph}(V,T_i,T_e), \quad (1)$$

where T_i is the lattice temperature, T_e is the electron temperature, V is the volume of the crystal, $E_0(V)$ is the static energy of the crystal at $T_i = T_e = 0$, F_e is the thermal free energy of the electronic excitations, and F_{ph} is the phonon free energy $F_e(V,0) = 0$. We deliberately introduced the electronic and ionic temperatures, because earlier a strong influence of the electronic temperature on the phonon spectrum had been established [13]. Both E_0 and F_e can be evaluated from DFT calculations directly. The phonon vibrational contribution F_{ph} can be expressed as

$$F_{ph}(V,T_i,T_e) = \frac{1}{2}\sum_{\mathbf{q}\lambda}\hbar\omega_{\mathbf{q}\lambda}(V,T_e) + k_B T_i \sum_{\mathbf{q}\lambda}\ln[1-\exp(-\hbar\omega_{\mathbf{q}\lambda}(V,T_e)/k_B T_i)], \quad (2)$$

where k_B is the Boltzmann constant and $\omega_{\mathbf{q}\lambda}$ is the phonon frequency of a mode λ at some $\mathbf{q}$ point.

According to the Lindemann criterion, melting starts when the ratio of the amplitude of thermal vibrations u to the average interatomic distance d_{nn} reaches some critical value L, which is called the Lindemann constant:

$$\sqrt{\langle u^2(T_m)\rangle} = L d_{nn}. \quad (3)$$

This equation determines the melting temperature.

The mean square displacement of the atoms can be directly calculated from the phonon spectrum [26]:

$$\langle u^2(T)\rangle = \frac{\hbar}{2M_a N}\sum_{\mathbf{q},\lambda}\frac{\coth(\hbar\omega_{\mathbf{q}\lambda}/2k_B T)}{\omega_{\mathbf{q}\lambda}}, \quad (4)$$

where M_a is the atomic mass, and N is the number of atoms in the crystal. Using the definition of the PhDOS,

$$g(\omega) = \frac{1}{N}\sum_{\mathbf{q},\lambda}\delta(\omega - \omega_{\mathbf{q}\lambda}), \quad (5)$$

the mean square displacement $\langle u^2(T)\rangle$ can be written as

$$\langle u^2(T)\rangle = \frac{\hbar}{2M_a}\int_0^\infty \frac{d\omega}{\omega} g(\omega)\coth\frac{\hbar\omega}{2k_B T}. \quad (6)$$

At a high temperature $T \approx T_m$ we can replace $\coth(\hbar\omega/2k_B T)$ by $2k_B T/\hbar\omega$. So using the Lindemann criterion (3) the melting temperature can be expressed from Eq. (6) as

$$T_m = \frac{(L d_{nn})^2}{k_B}\frac{M_a}{\langle\omega^{-2}\rangle}, \quad (7)$$

where

$$\langle\omega^{-2}\rangle = \int_0^\infty \frac{g(\omega)d\omega}{\omega^2}. \quad (8)$$

Obviously, the average interatomic distance is proportional to the lattice parameter ($d_{nn} \sim a$). Thus, in the framework of the Lindemann theory, we can obtain the melting temperature of a crystal at a given lattice parameter a by averaging over the PhDOS:

$$T_m = T_{m0}\left(\frac{a}{a_0}\right)^2\frac{\langle\omega_0^{-2}\rangle}{\langle\omega^{-2}\rangle}, \quad (9)$$

where the parameters of the reference point are denoted by index 0. Naturally, we used the experimental melting temperature at atmospheric pressure as T_{m0}.

To take into account the influence of the electronic temperature on the melting curve, we made a series of first-principle calculations of $F_e(V = \text{const}, T_e)$ with a 500 K electronic

temperature step and then interpolated the calculated points. We then iteratively solved Eq. (9) to get $T_m = T_i = T_e$. The pressure at this point is obtained by differentiation of the Helmholtz free energy (1) by volume at constant $T_i = T_e = T_m$:

$$P = -\left(\frac{\partial F(V,T_i,T_e)}{\partial V}\right)_{T=T_m}. \quad (10)$$

Thus the only empiric information in our calculations was the melting temperature at atmosphere pressure. This is not a restriction of our method, as we could choose the reference point from *ab initio* calculations. The following values of the melting temperature at atmospheric pressure were taken: 933.5 K for Al, 1358 K for Cu, and 1728 K for Ni [40].

Using Eq. (7) we estimated the Lindemann parameters for all the metals. As the average interatomic distance we took a doubled Wigner-Seitz radius $d_{at} = (6V_{at}/\pi)^{1/3}$. We obtained $L = 0.12$ for Al and Cu and $L = 0.11$ for Ni; these values are typical for fcc metals (0.1–0.13) [11].

III. RESULTS

A. Thermal expansion

At first we performed a series of calculations of a linear thermal expansion coefficient α_L to determine the influence of different parameters on thermophysical properties

$$\alpha_L = \frac{1}{3V}\left(\frac{\partial V}{\partial T}\right)_P. \quad (11)$$

The equilibrium volume V at a given temperature T was obtained from the Gibbs free energy G at zero pressure:

$$G(T,P) = \min_V [F(V,T) + PV]. \quad (12)$$

The profound effect of an approximation of the exchange-correlation functional on the thermal expansion of d elements was noted by Souvatzis and Eriksson [43]. They showed that the local density approximation (LDA) gave significantly lower values of α_L for $4d$ elements than the GGA; in some cases the LDA agreed better with experimental data up to 300 K. We calculated the thermal expansion curves of Al, Cu, and Ni up to melting; they are presented in Figs. 1–3. As can be seen from these figures, the GGA overestimates the thermal expansion for Al and Cu but underestimates it for Ni. The GGA shows better agreement with the experimental curve for Cu than the LDA. Figure 2 also demonstrates that the addition of six extra valence electrons for Cu has only a slight influence on the result. The experimental curves for Ni (see Fig. 3) have a distinct peak at the Curie temperature (≈628 K) which is not reproduced by our calculation. It is not surprising because we did not simulate the ionic motion directly. The spin polarization effects can be neglected for the thermal expansion coefficient as our results are very close for parallel, antiparallel, and zero spins (see Fig. 3). As for ferromagnetic properties, the calculated magnetic moment at 300 K coincides with the experimental value 0.62 μ_B/atom [40] (μ_B is the Bohr magneton).

It was shown by Grabowski *et al.* [44] that better agreement with experimental data can be obtained for Al by accounting of the electronic excitations as well as the effects of anharmonicity and vacancies. The influence of anharmonicity on thermodynamic properties of a number of metals (including Al, Cu, and Ni) was investigated recently [45]. In this study we consider only the electronic excitation; this can be justified by the good correspondence of the melting density to the experimental value. The following densities at the beginning of melting at atmospheric pressure were obtained: 2.49 g/cm^3 for Al, 8.03 g/cm^3 for Cu, and 8.43 g/cm^3 for Ni. The experimental values of solid-liquid densities at melting temperature and atmospheric pressure are: 2.56–2.38 g/cm^3 for Al [46], 8.35–7.95 g/cm^3 for Cu [47], and 8.21–7.82 g/cm^3 for Ni [42].

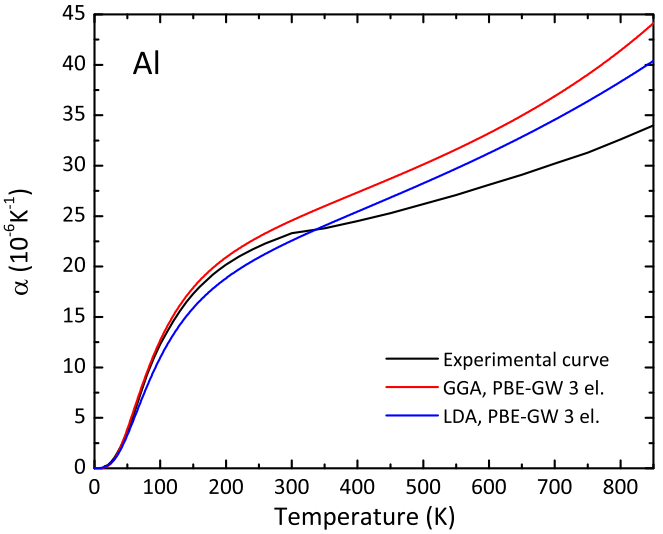

FIG. 1. (Color online) Linear expansion coefficient of Al. Red curve is the GGA exchange-correlation functional, blue curve is the LDA exchange-correlation functional, and the black line is an approximation of experimental data (Ref. [41]).

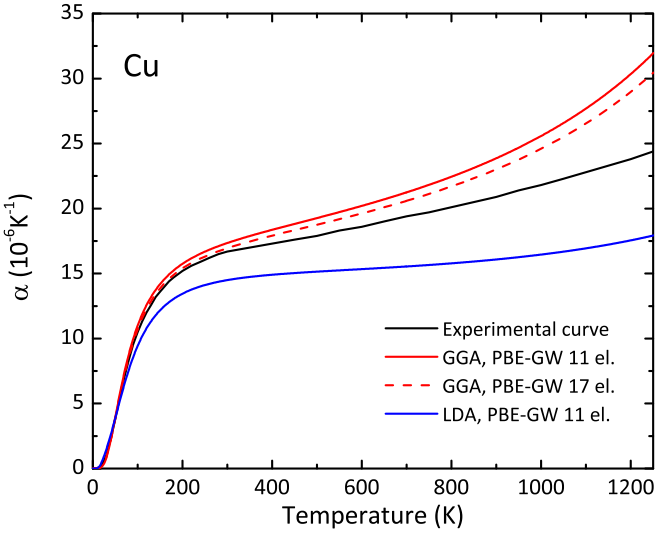

FIG. 2. (Color online) Linear expansion coefficient of Cu. Red curves are the GGA exchange-correlation functional (solid—11 valence electrons, dashed—17 valence electrons), blue curve is the LDA exchange-correlation functional, and the black line is an approximation of experimental data (Ref. [41]).

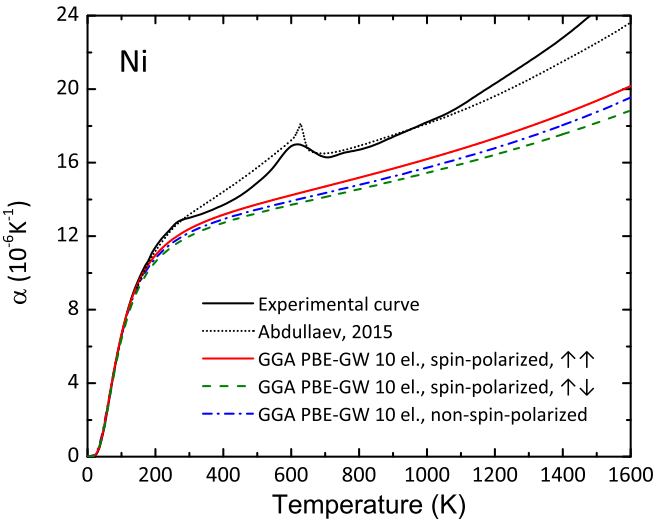

FIG. 3. (Color online) Linear expansion coefficient of Ni. Red curve is the GGA exchange-correlation functional with spin polarization (parallel spins), dashed green curve is the GGA exchange-correlation functional with spin polarization (antiparallel spins), dash-dotted blue curve is the GGA exchange-correlation functional without spin polarization, black line is an approximation of experimental data (Ref. [41]) until 1974, and the dotted black line is the experimental data (Ref. [42]).

B. Melting curves

The melting curve of Al is presented in Fig. 4. Our calculation shows excellent agreement both with the laser-heated diamond anvil cell (LHDAC) measurements [50–52] and the shock wave [53] experimental data. We also made a comparison with the first-principles melting curve obtained by the direct calculation of the free energies of both phases [48] and by the two-phase QMD approach [49]. In fact the melting

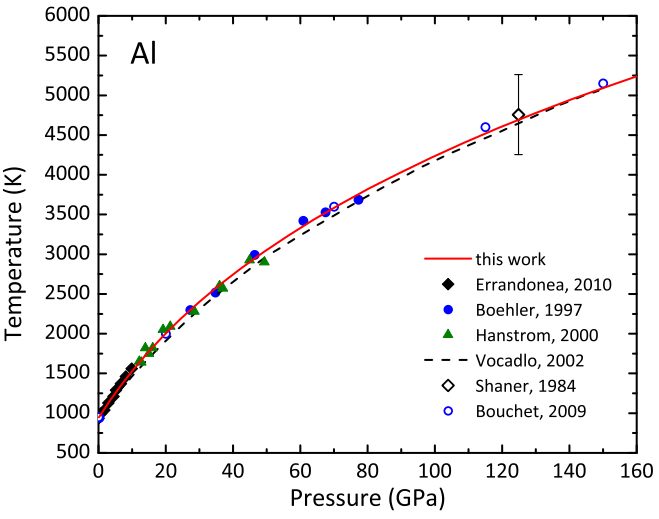

FIG. 4. (Color online) Melting curve of Al on the temperature-pressure diagram. Calculation: solid red line—current work, dashed black line—Ref. [48], and open blue circles—Ref. [49]. LHDAC: solid black diamonds—Ref. [50], solid blue circles—Ref. [51], and green triangles—Ref. [52]. Shock melting: open black diamonds—Ref. [53].

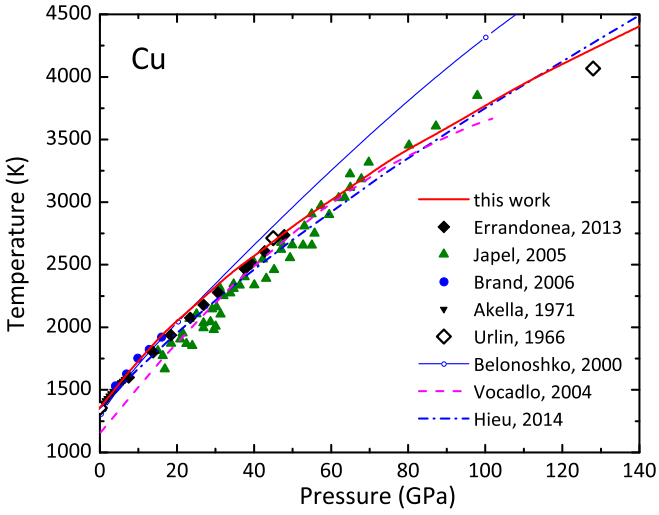

FIG. 5. (Color online) Melting curve of Cu on the temperature-pressure diagram. Calculation: solid red line—current work, dashed magenta line—Ref. [54], solid blue line with empty circles—Ref. [55], and dash-dotted blue line—Ref. [56]. LHDAC: solid black diamonds—Ref. [57], green triangles—Ref. [58], and solid blue circles—Ref. [59]. High pressure cavity: down black triangles—Ref. [60]. Melting curve from shock-wave data: open black diamond—Ref. [61].

curve of Al was calculated by many authors [2,68–74] using different techniques, and in most cases the results are in good agreement with the experiments.

Figure 5 shows the pressure dependence of the melting temperature of Cu. The curve of this work is in good correspondence with the high-pressure cavity [60] and LHDAC experimental data [57–59]. We also note that the first-principle results [54], and especially the statistical moment method [56], are very close to the curve of this work. On the other hand, the classical molecular dynamics [55] shows significantly higher melting temperatures at $P > 30$ GPa.

The melting curve of Ni is presented in Fig. 6. As can be immediately seen, there is a strong discrepancy among different models and experiments. Our approach agrees well with the first-principle curve of Pozzo and Alfé [65], the shock-induced melting from molecular dynamics [62], and the melting curve reconstruction from shock-wave experimental data [61]. The two-phase classical molecular dynamics simulations [64] give considerably higher temperatures on the melting curve. On the contrary, the statistical moment method [56] shows lower temperatures and agrees with the high-pressure cavity experiment [66]. However, none of these calculations describe the LHDAC experimental data [57,58,67]. We will discuss a peculiar situation with the Ni melting curve in Sec. IV. We should stress here that in the approach of this work, the non-spin-polarized calculation overestimates the melting temperature of Ni at high pressures (see the dashed red line in Fig. 6). For the spin-polarized calculation of the melting curve, the total spin was set to zero.

C. Melting temperature of crystals with excited electrons

With the dependence of the PhDOS on T_e it becomes possible to estimate the melting temperature of a crystal

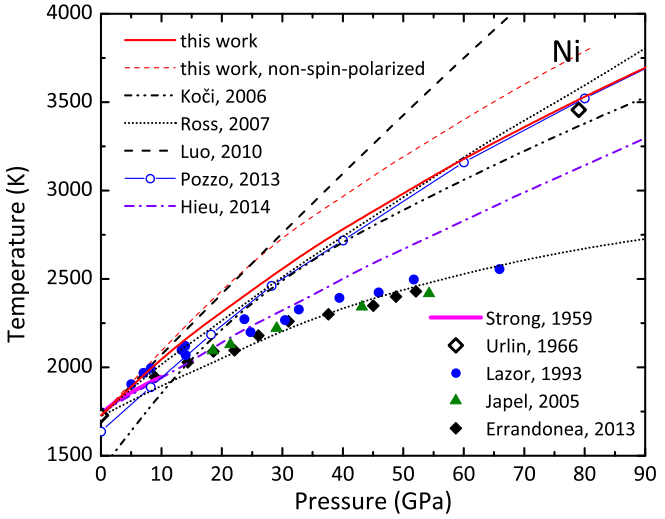

FIG. 6. (Color online) Melting curve of Ni on the temperature-pressure diagram. Calculation: solid red line (spin-polarized)—current work, dashed red line (non-spin-polarized)—current work, dash-double-dotted black line—Ref. [62], dotted black lines [model calculations with (lower) and without (upper) clusters]—Ref. [63], dashed black line—Ref. [64], solid blue line with open circles—Ref. [65], and dash-dotted violet line—Ref. [56]. High-pressure cavity: solid magenta line—Ref. [66]. LHDAC: solid blue circles—Ref. [67], green triangles—Ref. [58], and solid diamonds—Ref. [57]. Melting curve from shock-wave data: open black diamond—Ref. [61].

with the heated electrons. A strong influence of the electron temperature on the phonon properties of compressed Al, Cu, and Ni crystals can be seen in Figs. 7–9 where the PhDOS curves at different electron temperatures are presented. It is interesting to note the different behavior of the transverse low-frequency branch of the spectra at the increase of T_e: For Al the first maximum moves to the left, while for Cu and Ni it moves to the right. The longitudinal branch (second maximum) shifts to higher frequencies for all the metals under study. It should be noted that there is a drastic change of the shape of the transverse branch of the PhDOS of Ni between 0.04 and 0.43 eV (see Fig. 9).

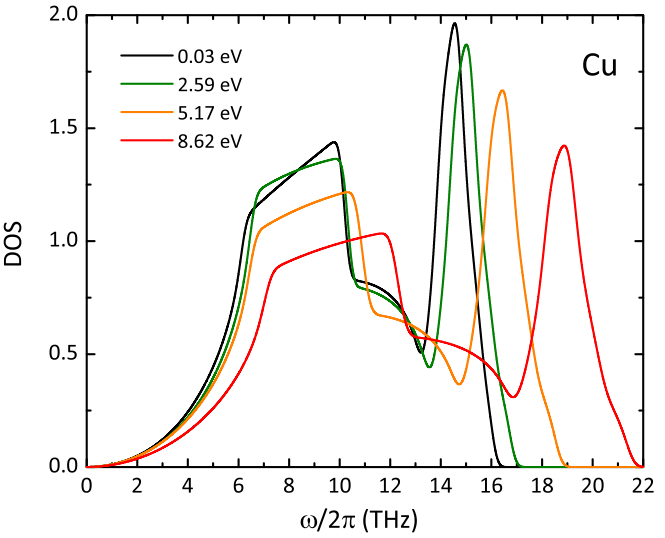

FIG. 8. (Color online) PhDOS for compressed Cu ($\rho = 1.55\rho_0$) at different electron temperatures.

Under femtosecond laser heating it is possible to create a nonequilibrium two-temperature state of a crystal with the cold lattice and hot electrons [75]. The existence time of such a system is determined by an electron-phonon coupling parameter γ; the dependence of this parameter on the electronic temperature can be significantly different: For Al and Cu γ rises with T_e, while for Ni it drops to rather low values [14,18]. Thermodynamic and transport properties of the crystal with the heated electrons may be significantly different from the equilibrium case [13,15–17,19,20]; this could influence the evolution of matter during the femtosecond laser heating. In Figs. 10–12 we demonstrate the dependence of the melting

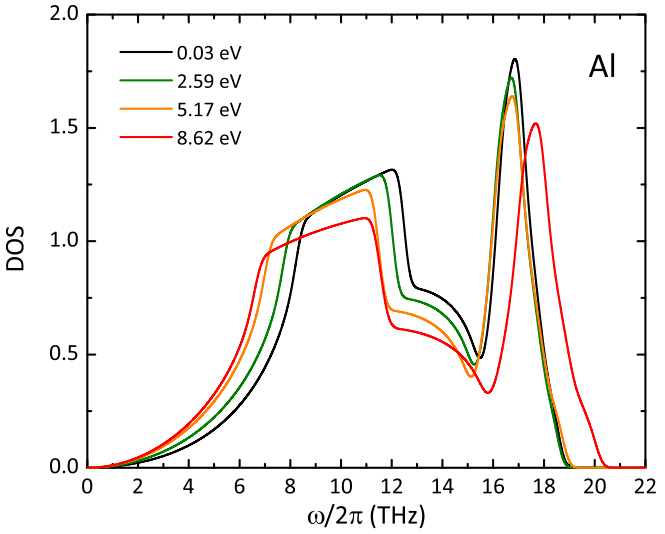

FIG. 7. (Color online) PhDOS for compressed Al ($\rho = 1.56\rho_0$) at different electron temperatures.

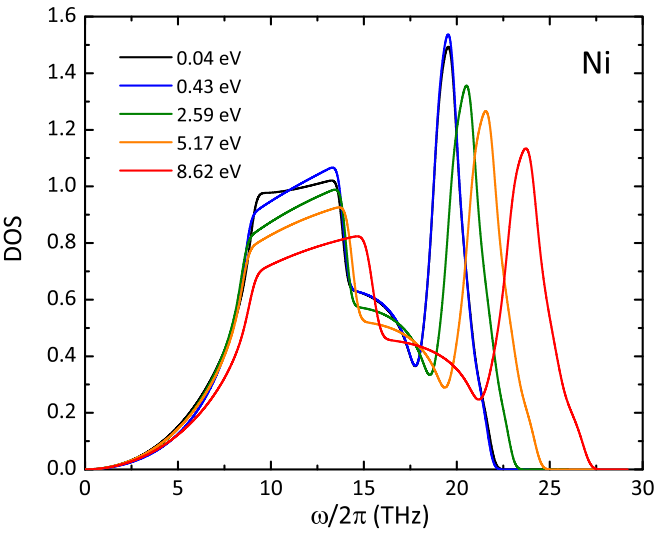

FIG. 9. (Color online) PhDOS for compressed Ni ($\rho = 1.67\rho_0$) at different electron temperature.

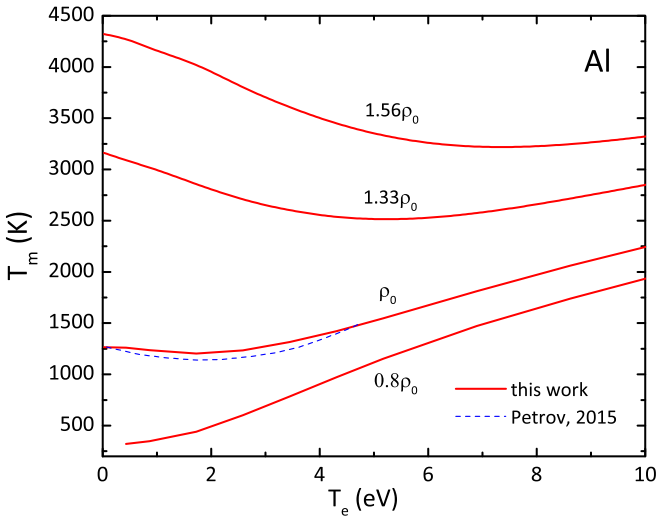

FIG. 10. (Color online) The melting temperature of Al at $\rho = 0.8\rho_0$, ρ_0, $1.33\rho_0$, and $1.56\rho_0$ vs the electron temperature. Solid lines—this work, dashed line—Ref. [80].

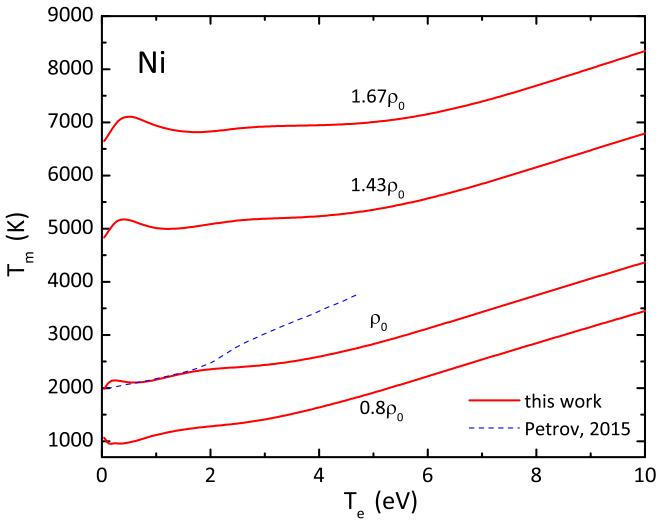

FIG. 12. (Color online) The melting temperature of Ni at $\rho = 0.8\rho_0$, ρ_0, $1.43\rho_0$, and $1.67\rho_0$ vs the electron temperature. Solid lines—this work, dashed line—Ref. [80].

temperature of Al, Cu, and Ni on the electron temperature. It is important to note that the melting temperature of the crystal at normal density is higher than that at normal pressure (the density in the last case is lower because of the thermal expansion). For example, at the same value of the Lindemann parameter, for Al the melting temperature at normal density is 1.27 kK, and a multiphase equation of state [76] gives 1.25 kK [77]. We investigated the crystals at normal, one lower, and two higher densities. The normal density ρ_0 was determined from the thermal expansion calculation to correspond to the temperature of 293 K. The following densities were obtained: 2.66 g/cm^3 for Al, 8.67 g/cm^3 for Cu, and 8.92 g/cm^3 for Ni. Our values agree well with previous calculations [78,79]. The corresponding experimental densities are: 2.7 g/cm^3 for Al, 8.96 g/cm^3 for Cu, and 8.9 g/cm^3 for Ni [40]. We observe the nonmonotonic behavior of the melting temperature for all the metals under study, but there is some considerable distinction in the curves for the compressed samples. As can be seen from Fig. 10, for compressed Al there is an explicit minimum of the melting temperature which moves to higher electron temperatures with the increase of the compression ratio. Compressed Cu demonstrates the nonmonotonic dependence of the melting temperature at $T_e < 4$ eV (see Fig. 11); at $T_e = 4 \div 10$ eV the melting temperature increases more than 1.5 times. The curves of the melting temperature for Ni have a pronounced local maximum at $\rho \geqslant \rho_0$ and $T_e < 0.5$ eV even at normal density (see Fig. 12). The dependence of the melting temperature of Ni at $T_e > 4$ eV is similar to that of Cu, but the rise of T_m is less significant.

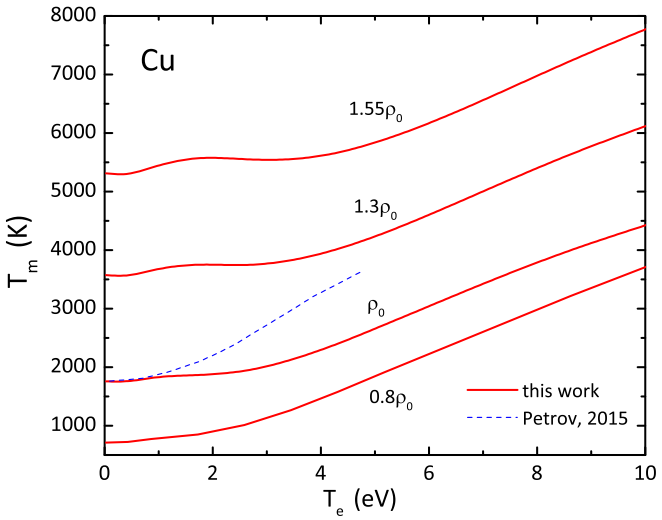

FIG. 11. (Color online) The melting temperature of Cu at $\rho = 0.8\rho_0$, ρ_0, $1.3\rho_0$, and $1.55\rho_0$ vs the electron temperature. Solid lines—this work, dashed line—Ref. [80].

It is also important that the melting temperature increases with T_e even for expanded metastable crystals (see curves for $\rho = 0.8\rho_0$ in Figs. 10–12; note that Al is unstable at $0.8\rho_0$ and $T_e < 0.4$ eV). This fact simplifies an experimental investigation of melting under femtosecond laser heating.

Dependences of the melting curves of a number of metals on the electronic temperature were estimated recently [80] using the approach similar to that of Ref. [13]. The elastic moduli and the Debye temperature Θ_D were computed, and then the melting temperature at a given T_e was determined from a simple scaling criterion $T_m(T_e) \propto \Theta_D^2(T_e)$. The resulting curves are also shown in Figs. 10–12 by the dashed lines. It is clearly seen that only for Al the model [80] demonstrates good agreement with our approach; for Cu and Ni the curves are monotonic, and the melting temperature is significantly overestimated.

IV. DISCUSSION

We have demonstrated the applicability of the QA and the Lindemann criterion for the reconstruction of melting curves of Al, Cu, and Ni up to Mbar pressures. However, it is important to analyze the factors we neglected in our approach. The influence of anharmonicity can be considerable for some crystals; additional calculations may be necessary

to determine the anharmonic contribution to the free energy [24,25,44,45,81,82]. Although our calculations for Al and Cu agree well with static and dynamic experimental data, for Ni, however, there is a strong difference between our melting curve and the LHDAC experimental points. On the other hand, these points still have not been confirmed by any first-principle or molecular dynamic method. In fact, the LHDAC points were only reproduced by the free energy model of melting with the account of clusters by Ross *et al.* [63]. It is interesting that the free energy model calculations without clusters are close to the shock-wave data and agree well with the *ab initio* approach of Pozzo and Alfé [65] as well as with our curve.

Actually the problem of the strong discrepancy between LHDAC and shock-wave experimental data manifests itself not only for Ni but also for some other metals, in particular for molybdenum [83,84], tantalum [83,85], and iron [83,86,87]. The first-principle calculations [88,89] for these cases are systematically closer to shock-wave data. So it is a remarkable fact that a recent LHDAC work, in which different diagnostics are proposed to identify the melting transition, seems to reconcile these differences for tantalum [90] and iron [91]. Thus additional experimental efforts are required to clarify the actual position of the melting curve of Ni.

Analyzing Figs. 10–12, we note the essential distinction between $T_m(T_e)$ for Al and two other metals. The drop of the melting temperature for the compressed Al can be explained by the weakening of the interatomic potential caused by the redistribution of the electronic density in the interstitial region. The complicated behavior of the electron density distribution is caused by the excitation of electrons; the corresponding densities of state and their temperature dependence for Al, Cu, and Ni can be found elsewhere [14,92]. In this connection it is interesting to analyze the nonmonotonic behavior of the melting temperature at $T_e < 0.5$ eV for Ni (see Fig. 12). The d band of this element is almost full at normal conditions, and the Fermi level almost coincides with the high-energy edge of the d band, so the density of states is very high at the Fermi level. The d electrons in this case are easily excited even at very low electron temperatures, therefore the abrupt change of the melting temperature is observed in Fig. 12 at low T_e.

The melting temperature of the crystals at $T_e = 10$ eV and normal density rises almost two times for Al and Ni and even more for Cu (see Figs. 10–12). This is a noticeable effect which can be registered experimentally. Indeed, it has been revealed recently [21] that a gold crystal becomes harder at the elevated electron temperature [21]. Earlier, using femtosecond laser diffraction the 1.5 times overheating of an Al crystal was registered [93] at 1.5 ps. The estimation of the electron temperature at this moment for the laser parameters (duration 120 fs, wavelength 775 nm, fluence 70 mJ/cm^2, and foil thickness 20 nm) gives [94] about 3 kK (the maximum value of T_e during the process does not exceed 1 eV). Figure 10 shows that at $T_e < 1$ eV the melting temperature of Al slightly decreases, therefore the hardening of the crystal cannot be discovered in this case.

In fact for the metals under study the hardening effect might be found experimentally in the case of sufficiently long existence of the two-temperature state. The main parameter defining the rate of exchange between a lattice and electrons is the electron-phonon relaxation time [18,95,96]. An extensive

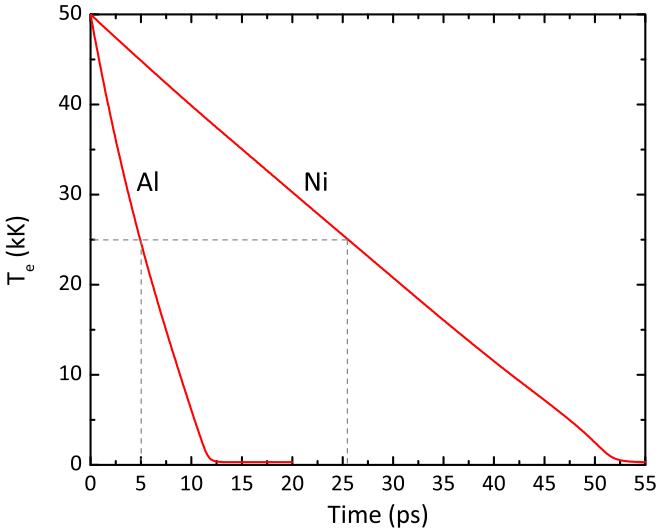

FIG. 13. (Color online) Electronic temperature relaxation for Al and Ni. The vertical dashed lines correspond to the estimation of the relaxation time.

study of the electron-phonon coupling parameter γ and the electron isochoric heat capacity C_e for a number of metals including Al, Cu, and Ni was carried out by Lin and Zhigilei [14]. They showed that the strength of the electron-phonon coupling increases essentially for Cu, increases slightly for Al, and decreases drastically for Ni at $T_e \leqslant 2$ eV. Petrov *et al.* [18] confirmed these inferences up to $T_e = 5$ eV using the improved model of electron-phonon coupling. We estimated the temperature relaxation time between the electrons and the lattice using the dependences $\gamma(T_e)$ from Ref. [18] and $C_e(T_e)$ from Ref. [92]. For this purpose we solved the temperature relaxation equation for T_e assuming only the relaxation process at some spatial point:

$$C_e \frac{dT_e}{dt} = -\gamma(T_e)(T_e - T_l), \tag{13}$$

with the initial condition $T_e(0) = 50$ kK. Here $T_l = 300$ K is the constant temperature of the lattice. The time evolution of the electronic temperature $T_e(t)$ according to Eq. (13) for Al and Ni are presented in Fig. 13.

The relaxation time was estimated at the twofold decrease of the electronic temperature (25 kK); it turned out to be ~5 ps for Al and ~25 ps for Ni. It is interesting to note that at a constant value of $\gamma = 10.5 \times 10^{17}$ W m^{-3} K^{-1} for Ni [97], the relaxation time is estimated as only ~5 ps. Therefore the account of the decreasing dependence of $\gamma(T_e)$ for Ni significantly enhances the lifetime of the two-temperature state.

The obtained relaxation times are upper-bound estimates as other important effects are neglected. To be specific, we consider a bulk target irradiated by a femtosecond laser pulse. The laser radiation is absorbed in the skin layer of the target by the conduction band electrons, and then this energy is distributed to the electrons in the deeper regions of the target (through the electronic heat conduction) and to the ions (by the electron-phonon exchange mechanism). Emission of electrons from the target surface is negligible as the escaped

electrons form a cloud which prevents other electrons from leaving the target [98]. The thermal conductivity coefficient of metals is rather high (237 W/(m K) for Al, 401 W/(m K) for Cu) [40] and increases with T_e [18]. The speed of the thermal wave is on the order of $\sqrt{\chi/t}$ (where χ is the thermal diffusivity). For example, for aluminum at $t = 2$ ps the estimated speed of the thermal wave is about 7 km/s, which is significantly faster than the sound velocity. In this case the electronic temperature of inner layers of the target may become significant while the ions remain cold during some time. On the other hand, heating of electrons leads to the rise of pressure which at $T_e = 10$ eV can reach several megabars (about 4 Mbars for Ni) and causes the expansion of the target in the direction opposite to the propagation of the laser pulse [99]. Thus some inner layers of the target may experience almost isochoric melting at heated electrons [76], and the effect of crystal hardening may influence the evolution of the target material.

To directly register the effect of hardening of a thin golden foil, a femtosecond electron diffraction technique is used to study the time evolution of Bragg peaks [100]. The main problem of this setup is the heterogeneous melting of the foil from its surfaces due to the expansion of the foil under the action of high electronic pressure. As the hardening effect is valid even at $0.8\rho_0$, it is possible to suppress the heterogeneous melting by placing a transparent (glass or sapphire) layer in front of the foil. The other experimental possibility is to measure the complex reflectivity of metals in pump-probe experiments [101] using optically thick targets. As the reflectivity of the liquid phase can be significantly lower than that of the solid phase (for example, for Al the difference is about 30% at the photon energy of 1 eV [102,103]), this effect might be registered at subpicosecond delays between the pump and probe pulses [104]. Obviously, at the crystal hardening the drop of reflectivity will occur later than expected. Again, to suppress the heterogeneous melting from the surface one might use a surrounding medium such as water environment or a solid overlayer.

V. CONCLUSION

Using the QA and the Lindemann criterion, we have calculated the melting curves of Al, Cu, and Ni up to megabar pressure. The plane-wave pseudopotential DFT code VASP was applied to accurately determine the electronic structure; then the PhDOS was determined by means of the PHONOPY package. We considered the dependence of the PhDOS on the electronic temperature; this dependence was implicitly taken into account at the computation of the phonon pressure, the linear thermal expansion coefficient, and the mean square displacement of atoms. Our dependencies of the melting temperature on the pressure for Al and Cu revealed good agreement with the static and shock-wave experimental data. For Ni the spin polarization is important to reproduce the recent first-principle simulation of the melting curve and the shock-wave data; on the other hand, the LHDAC melting temperatures are situated significantly below our curve. The PhDOS curves of the crystals at different electronic temperatures are sensitive to the peculiarities of the electronic structure. This leads to the complex nonmonotonic dependences of the melting temperature on the electronic one. Nevertheless, for all three metals at normal density the melting temperature at $T_e = 10$ eV rises significantly, thus indicating the hardening of the crystal lattice. This effect might be discovered experimentally as the lifetime of the two-temperature state is at least several picoseconds.

ACKNOWLEDGMENTS

We thank Dr. N. Smirnov, Dr. M. Povarnitsyn and Prof. Yu. Petrov for useful discussions and advice. The majority of computations, development of codes, and treatment of results were carried out in the Joint Institute for High Temperatures RAS under financial support of the Russian Science Foundation (Grant No. 14-50-00124). Some numerical calculations were performed free of charge on supercomputers of Moscow Institute of Physics and Technology and Tomsk State University.

[1] Y. Zhang and E. J. Maginn, J. Chem. Phys. **136**, 144116 (2012).
[2] J. R. Morris, C. Z. Wang, K. M. Ho, and C. T. Chan, Phys. Rev. B **49**, 3109 (1994).
[3] G. Grimvall, B. Magyari-Köpe, V. Ozoliņš, and K. A. Persson, Rev. Mod. Phys. **84**, 945 (2012).
[4] F. A. Lindemann, Physik. Zeitschr. **11**, 609 (1910).
[5] J. J. Gilvarry, Phys. Rev. **102**, 308 (1956).
[6] M. Ross, Phys. Rev. **184**, 233 (1969).
[7] F. E. Simon and G. Glatzel, Z. Anorg. Allgem. Chem. **178**, 309 (1929).
[8] E. A. Kraut and G. C. Kennedy, Phys. Rev. **151**, 668 (1966).
[9] W. G. Hoover and M. Ross, Contemp. Phys. **12**, 339 (1971).
[10] S. M. Stishov, Phys. Usp. **17**, 625 (1975).
[11] G. Grimvall, Sci. Model. Simul. **15**, 21 (2008).
[12] G. H. Wolf and R. Jeanloz, J. Geophys. Res. **89**, 7821 (1984).
[13] V. Recoules, J. Clérouin, G. Zérah, P. M. Anglade, and S. Mazevet, Phys. Rev. Lett. **96**, 055503 (2006).
[14] Z. Lin, L. V. Zhigilei, and V. Celli, Phys. Rev. B **77**, 075133 (2008).
[15] P. R. Levashov, G. V. Sin'ko, N. A. Smirnov, D. V. Minakov, O. P. Shemyakin, and K. V. Khishchenko, J. Phys. Condens. Matter **22**, 505501 (2010).
[16] G. Norman, I. Saitov, V. Stegailov, and P. Zhilyaev, Contrib. Plasma Phys. **53**, 300 (2013).
[17] Y. Petrov and N. Inogamov, JETP Lett. **98**, 278 (2013).
[18] Y. Petrov, N. Inogamov, and K. Migdal, JETP Lett. **97**, 20 (2013).
[19] D. V. Knyazev and P. R. Levashov, Phys. Plasmas **21**, 073302 (2014).
[20] D. V. Knyazev and P. R. Levashov, Phys. Plasmas **22**, 053303 (2015).
[21] R. Ernstorfer, M. Harb, C. T. Hebeisen, G. Sciaini, T. Dartigalongue, and R. J. D. Miller, Science **323**, 1033 (2009).
[22] Y. Giret, S. L. Daraszewicz, D. M. Duffy, A. L. Shluger, and K. Tanimura, Phys. Rev. B **90**, 094103 (2014).

[23] F. Luo, L.-C. Cai, X.-R. Chen, F.-Q. Jing, and D. Alfè, J. Appl. Phys. **111**, 053503 (2012).
[24] S. Xiang, F. Xi, Y. Bi, J. Xu, H. Geng, L. Cai, F. Jing, and J. Liu, Phys. Rev. B **81**, 014301 (2010).
[25] D. Cebulla and R. Redmer, Phys. Rev. B **89**, 134107 (2014).
[26] T. Yildirim and A. B. Harris, Phys. Rev. B **46**, 7878 (1992).
[27] S. V. Lepeshkin, M. V. Magnitskaya, and E. G. Maksimov, JETP Lett. **89**, 586 (2009).
[28] D. M. Medvedev and Yu. V. Petrov, J. Exp. Theor. Phys. **88**, 128 (1999).
[29] G. Kresse and J. Hafner, Phys. Rev. B **47**, 558 (1993).
[30] G. Kresse and J. Hafner, Phys. Rev. B **49**, 14251 (1994).
[31] G. Kresse and J. Furthmüller, Phys. Rev. B **54**, 11169 (1996).
[32] G. Kresse and J. Furthmüller, Comput. Mater. Sci. **6**, 15 (1996).
[33] A. Togo, F. Oba, and I. Tanaka, Phys. Rev. B **78**, 134106 (2008).
[34] X. Gonze and C. Lee, Phys. Rev. B **55**, 10355 (1997).
[35] J. P. Perdew, K. Burke, and M. Ernzerhof, Phys. Rev. Lett. **77**, 3865 (1996).
[36] J. P. Perdew, K. Burke, and M. Ernzerhof, Phys. Rev. Lett. **78**, 1396 (1997).
[37] G. Kresse and D. Joubert, Phys. Rev. B **59**, 1758 (1999).
[38] M. Shishkin and G. Kresse, Phys. Rev. B **74**, 035101 (2006).
[39] H. J. Monkhorst and J. D. Pack, Phys. Rev. B **13**, 5188 (1976).
[40] *CRC Handbook of Chemistry and Physics, Internet Version 2005*, edited by D. R. Lide (CRC Press, Boca Raton, FL, 2005).
[41] S. I. Novikova, *Thermal expansion of solids* (in Russian) (Nauka, Moscow, 1974).
[42] R. Abdullaev, Y. Kozlovskii, R. Khairulin, and S. Stankus, Int. J. Thermophys. **36**, 603 (2015).
[43] P. Souvatzis and O. Eriksson, Phys. Rev. B **77**, 024110 (2008).
[44] B. Grabowski, L. Ismer, T. Hickel, and J. Neugebauer, Phys. Rev. B **79**, 134106 (2009).
[45] A. Glensk, B. Grabowski, T. Hickel, and J. Neugebauer, Phys. Rev. Lett. **114**, 195901 (2015).
[46] C. E. Birchenall, A. J. Harrison, and S. N. Balart, Metall. Trans. A **11**, 1213 (1980).
[47] *Asm Handbook: Properties and Selection: Nonferrous Alloys and Special-Purpose Materials*, Vol. 2, 10th ed. (ASM International, Materials Park, OH, 1990).
[48] L. Vočadlo and D. Alfè, Phys. Rev. B **65**, 214105 (2002).
[49] J. Bouchet, F. Bottin, G. Jomard, and G. Zérah, Phys. Rev. B **80**, 094102 (2009).
[50] D. Errandonea, J. Appl. Phys. **108**, 033517 (2010).
[51] R. Boehler and M. Ross, Earth Planet. Sci. Lett. **153**, 223 (1997).
[52] A. Hänström and P. Lazor, J. Alloys Compd. **305**, 209 (2000).
[53] J. W. Shaner, J. M. Brown, and R. G. McQueen, *High Pressure in Science and Technology* (North Holland, Amsterdam, 1984).
[54] L. Vocadlo, D. Alfe, G. D. Price, and M. J. Gillan, J. Chem. Phys. **120**, 2872 (2004).
[55] A. B. Belonoshko, R. Ahuja, O. Eriksson, and B. Johansson, Phys. Rev. B **61**, 3838 (2000).
[56] H. K. Hieu, J. Appl. Phys. **116**, 163505 (2014).
[57] D. Errandonea, Phys. Rev. B **87**, 054108 (2013).
[58] S. Japel, B. Schwager, R. Boehler, and M. Ross, Phys. Rev. Lett. **95**, 167801 (2005).
[59] H. Brand, D. P. Dobson, L. Vočadlo, and I. G. Wood, High Press. Res. **26**, 185 (2006).
[60] J. Akella and G. C. Kennedy, J. Geophys. Res. **76**, 4969 (1971).
[61] V. D. Urlin, Sov. Phys. JETP **22**, 341 (1966).
[62] L. Koči, E. M. Bringa, D. S. Ivanov, J. Hawreliak, J. McNaney, A. Higginbotham, L. V. Zhigilei, A. B. Belonoshko, B. A. Remington, and R. Ahuja, Phys. Rev. B **74**, 012101 (2006).
[63] M. Ross, R. Boehler, and D. Errandonea, Phys. Rev. B **76**, 184117 (2007).
[64] F. Luo, X.-R. Chen, L.-C. Cai, and G.-F. Ji, J. Chem. Eng. Data **55**, 5149 (2010).
[65] M. Pozzo and D. Alfè, Phys. Rev. B **88**, 024111 (2013).
[66] H. M. Strong and F. P. Bundy, Phys. Rev. **115**, 278 (1959).
[67] P. Lazor, G. Shen, and S. Saxena, Phys. Chem. Miner. **20**, 86 (1993).
[68] J. A. Moriarty, D. A. Young, and M. Ross, Phys. Rev. B **30**, 578 (1984).
[69] J. Mei and J. W. Davenport, Phys. Rev. B **46**, 21 (1992).
[70] G. A. de Wijs, G. Kresse, and M. J. Gillan, Phys. Rev. B **57**, 8223 (1998).
[71] B. J. Jesson and P. A. Madden, J. Chem. Phys. **113**, 5924 (2000).
[72] D. Alfè, Phys. Rev. B **68**, 064423 (2003).
[73] I. Lomonosov, Laser Part. Beams **25**, 567 (2007).
[74] G. Robert, P. Legrand, P. Arnault, N. Desbiens, and J. Clérouin, Phys. Rev. E **91**, 033310 (2015).
[75] S. I. Anisimov, B. L. Kapeliovich, and T. L. Perel'man, Sov. Phys. JETP **39**, 375 (1974).
[76] M. E. Povarnitsyn, T. E. Itina, M. Sentis, K. V. Khishchenko, and P. R. Levashov, Phys. Rev. B **75**, 235414 (2007).
[77] P. A. Krasnova and P. R. Levashov, Int. J. Heat Mass Transfer **83**, 311 (2015).
[78] B. Grabowski, T. Hickel, and J. Neugebauer, Phys. Rev. B **76**, 024309 (2007).
[79] A. D. Corso, J. Phys. Condens. Matter **25**, 145401 (2013).
[80] Y. Petrov, K. Migdal, N. Inogamov, and V. Zhakhovsky, Appl. Phys. B **119**, 401 (2015).
[81] Z. Wu, Phys. Rev. B **81**, 172301 (2010).
[82] B. Grabowski, P. Söderlind, T. Hickel, and J. Neugebauer, Phys. Rev. B **84**, 214107 (2011).
[83] D. Errandonea, B. Schwager, R. Ditz, C. Gessmann, R. Boehler, and M. Ross, Phys. Rev. B **63**, 132104 (2001).
[84] R. S. Hixson, D. A. Boness, J. W. Shaner, and J. A. Moriarty, Phys. Rev. Lett. **62**, 637 (1989).
[85] C. Dai, J. Hu, and H. Tan, J. Appl. Phys. **106**, 043519 (2009).
[86] C. S. Yoo, N. C. Holmes, M. Ross, D. J. Webb, and C. Pike, Phys. Rev. Lett. **70**, 3931 (1993).
[87] J. H. Nguyen and N. C. Holmes, Nature (London) **427**, 339 (2004).
[88] S. Taioli, C. Cazorla, M. J. Gillan, and D. Alfè, Phys. Rev. B **75**, 214103 (2007).
[89] D. Alfè, Phys. Rev. B **79**, 060101 (2009).
[90] A. Dewaele, M. Mezouar, N. Guignot, and P. Loubeyre, Phys. Rev. Lett. **104**, 255701 (2010).
[91] S. Anzellini, A. Dewaele, M. Mezouar, P. Loubeyre, and G. Morard, Science **340**, 464 (2013).
[92] E. Bévillon, J. P. Colombier, V. Recoules, and R. Stoian, Phys. Rev. B **89**, 115117 (2014).
[93] B. J. Siwick, J. R. Dwyer, R. E. Jordan, and R. J. D. Miller, Science **302**, 1382 (2003).
[94] http://vll.ihed.ras.ru.
[95] Y. Petrov, Laser Part. Beams **23**, 283 (2005).

[96] N. A. Inogamov, V. V. Zhakhovsky, Y. V. Petrov, V. Khokhlov, S. I. Ashitkov, K. V. Khishchenko, K. P. Migdal, D. K. Ilnitsky, Y. N. Emirov, P. S. Komarov, V. V. Shepelev, C. Miller, I. Oleynik, M. Agranat, A. Andriyash, S. Anisimov, and V. Fortov, Contrib. Plasma Phys. **53**, 796 (2013).

[97] P. Caffrey, P. E. Hopkins, J. M. Klopf, and P. M. Norris, Microscale Thermophys. Eng. **9**, 365 (2005).

[98] D. M. Riffe, X. Y. Wang, M. C. Downer, D. L. Fisher, T. Tajima, J. L. Erskine, and R. M. More, J. Opt. Soc. Am. B **10**, 1424 (1993).

[99] M. E. Povarnitsyn, V. B. Fokin, and P. R. Levashov, Appl. Surf. Sci. **357**, 1150 (2015).

[100] S. L. Daraszewicz, Y. Giret, N. Naruse, Y. Murooka, J. Yang, D. M. Duffy, A. L. Shluger, and K. Tanimura, Phys. Rev. B **88**, 184101 (2013).

[101] R. Evans, A. D. Badger, F. Falliès, M. Mahdieh, T. A. Hall, P. Audebert, J.-P. Geindre, J.-C. Gauthier, A. Mysyrowicz, G. Grillon, and A. Antonetti, Phys. Rev. Lett. **77**, 3359 (1996).

[102] *Handbook of Optical Constants of Solids* (Academic, New York, 1985).

[103] L. Akashev and V. Kononenko, High Temp. **39**, 384 (2001).

[104] M. Kandyla, T. Shih, and E. Mazur, Phys. Rev. B **75**, 214107 (2007).